HHS Public Access

Author manuscript

Clin Cancer Res. Author manuscript; available in PMC 2017 January 01.

Published in final edited form as:

Clin Cancer Res. 2016 January 1; 22(1): 107–121. doi:10.1158/1078-0432.CCR-15-0235.

Integrating Murine and Clinical Trials with Cabozantinib to Understand Roles of MET and VEGFR-2 as Targets for Growth Inhibition of Prostate Cancer

Andreas Varkaris[1,†], **Paul G. Corn**[1,†], **Nila U. Parikh**[1], **Eleni Efstathiou**[1], **Jian H. Song**[1], **Yu-Chen Lee**[1,2], **Ana Aparicio**[1], **Anh G. Hoang**[1], **Sanchaika Gaur**[1,3], **Lynnelle Thorpe**[1,3], **Sankar N. Maity**[1], **Menashe Bar Eli**[3,4], **Bogdan A. Czerniak**[5], **Yiping Shao**[6], **Mian Alauddin**[7], **Sue-Hwa Lin**[1,2], **Christopher J. Logothetis**[1], and **Gary E. Gallick**[1,3,*]

[1]Department of Genitourinary Medical Oncology, David H. Koch Center for Applied Research of Genitourinary Cancers, The University of Texas, M.D. Anderson Cancer Center

[2]Department of Translational Molecular Pathology, The University of Texas, M.D. Anderson Cancer Center

[3]Programs in Cancer Biology and Cancer Metastasis, The University of Texas Graduate School of Biomedical Sciences at Houston

[4]Department of Cancer Biology, The University of Texas, M.D. Anderson Cancer Center

[5]Department of Pathology, The University of Texas, M.D. Anderson Cancer Center

[6]Department of Imaging Physics-Research, The University of Texas, M.D. Anderson Cancer Center

[7]Department of Cancer Systems Imaging, The University of Texas, M.D. Anderson Cancer Center

Abstract

Purpose—We performed parallel investigations in cabozantinib-treated patients in a Phase 2 trial and simultaneously in Patient-derived Xenograft (PDX) models to better understand the roles of MET and VEGFR-2 as targets for prostate cancer therapy.

Experimental Design—In the clinical trial, radiographic imaging and serum markers were examined, as well as molecular markers in tumors from bone biopsies. In mice harboring PDX intrafemurally or subcutaneously, cabozantinib effects on tumor growth, MET, PDX in which MET was silenced, VEGFR-2, bone turnover, angiogenesis and resistance were examined.

[*]To whom correspondence should be addressed: Gary E. Gallick, Ph.D., Department of Genitourinary Medical Oncology, The University of Texas MD Anderson Cancer Center, Clinical Research Building (T7.3891), 1515 Holcombe Blvd. Unit 0018-4 Houston, TX 77030, Phone: (713) 563-4919 ggallick@mdanderson.org.

[†]equal contribution

Conflict of interest disclosure statement: The authors have declared that no conflict of interest exists.

Author contributions: GEG, CJL, and AV conceived the study. AV, PGC, SL, YS, MA, GEG, and CJL and S-HL designed the study. AV, PGC, EE, JHS, NUP, Y-CL, AA, JZ, SNM, MBE and BAC were involved in the acquisition of data. Data analysis and interpretation were undertaken by AV, PC, BAC, SG, LT, S-HL, GEG and CJL. NUP and AGH provided technical support. CJL and GEG supervised the study. AV, PGC, CJL, and GEG and S-HL wrote the paper, which was reviewed by all authors. EE, AA, BC, JZ and SM were involved in the writing, reviewing, or both, of the paper.

Results—In responsive patients and PDX, islets of viable, p-MET-positive tumor cells persisted, which rapidly regrew after drug withdrawal. Knockdown of MET in PDX did not affect tumor growth in mice, nor did it affect cabozantinib-induced growth inhibition, but did lead to induction of FGFR-1. Inhibition of VEGFR-2 and MET in endothelial cells reduced the vasculature, leading to necrosis. However, each islet of viable cells surrounded a VEGFR-2-negative vessel. Reduction of bone turnover was observed in both cohorts.

Conclusion—Our studies demonstrate that MET in tumor cells is not a persistent therapeutic target for metastatic CRPC, but inhibition of VEGF-R2 and MET in endothelial cells and direct effects on osteoblasts are responsible for cabozantinib-induced tumor inhibition. However, vascular heterogeneity represents one source of primary therapy resistance, whereas induction of FGFR-1 in tumor cells suggests a potential mechanism of acquired resistance. Thus, integrated cross-species investigations demonstrate the power of combining preclinical models with clinical trials to understand mechanisms of activity and resistance of investigational agents.

Introduction

The planned integration of clinical and murine investigations can overcome the limitations of each and efficiently link mechanisms to therapeutic benefit. Further, this strategy can provide mechanistic insights into clinical observations (1–3). This approach is particularly relevant in cancers in which “drivers” that account for important clinical phenotypes have not been identified, such as bone metastatic castrate-resistant prostate cancer (mCRPC). This limited understanding of the biology of the disease and mechanisms of resistance hamper development of targeted therapeutic strategies for mCRPC. An example of the difficulty of objectively linking clinical observations to inhibition of specific signaling pathways has occurred with cabozantinib, an oral multi-kinase inhibitor with potent activity against MET and VEGFR-2 (4) which, in Phase 2 clinical trials, led to striking improvements in bone scans, associated with reduced pain and soft-tissue/visceral tumor responses and reduction in circulating tumor cells (5, 6). A major caveat of these studies is that the mechanisms leading to these responses, despite a corresponding decline in serum PSA, are not fully understood. Nevertheless, the initial excitement from cabozantinib responses led to a recent phase 3 clinical trial studying the effects of cabozantinib monotherapy in late stage mCRPC (COMET 1). This Phase 3 study showed a significant lengthening of progression free survival but not prolongation of overall survival compared to patients treated with prednisone (7).

The inability to prolong survival in a large-scale phase 3 clinical trial illustrates a central problem in therapy development. Neither preclinical models nor phase 1 and phase 2 clinical trials alone have been sufficient to predict success of novel therapies in phase 3 clinical trials. In mCRPC, serial sampling and molecular-pathologic analyses of tumors via trans-iliac bone marrow biopsies have facilitated the discovery of predictive biomarkers of response and resistance. However, an inherent problem with examining markers in human bone biopsies from prostate cancer patients in phase 2 clinical trials is intratumoral heterogeneity, both within individual biopsy samples and over time, leading to sampling bias (8–11). While preclinical models allow more complete examination of markers, they often overestimate the success of novel therapies. To overcome these limitations, we have

used the approach of running parallel investigations on well-defined, representative patient-derived xenografts (PDX) in conjunction with a phase 2 clinical trial as a strategy to provide insights into the unanticipated clinical findings. Studies in PDX are suited to defining mechanisms as they lack limitations as to the time course over which specimens can be collected and allow the collection of large amounts of material for analyses. In addition, PDX can be genetically manipulated to assess the effects of specific gene products on therapy response, thus allowing mechanistic studies on drug targets and resistance. For these reasons, mouse models complement clinical investigations.

Our parallel studies provided insights into the mechanism of action of cabozantinib that are of general relevance to targeted agents for the treatment of prostate cancer. Specifically, we demonstrate: (1) MET in tumor cells is not a sustained therapeutic target for established, late-stage tumors, but MET in the microenvironment is; (2) genetic and pharmacologic inhibition of MET leads to induction of FGFR-1 expression in tumor cells; (3) vascular heterogeneity represents one source of primary resistance when VEGFR-2 is targeted; (4) inhibition of osteoblast proliferation and induction of differentiation is responsible for the compelling bone scan changes in cabozantinib-treated patients and mice bearing PDX; and (5) biologically optimized dose and scheduling of therapy may be important for maximizing the efficacy of microenvironment-targeting agents.

Materials and Methods

Clinical trial

A multi-institutional, non-randomized expansion cohort for men with prostate cancer was added to a phase 2 randomized discontinuation study of cabozantinib in subjects with advanced solid tumors-NCT00940225 (the phase 2 trial was an Exelixis sponsored study) (6). Cabozantinib was administered orally at a daily starting dose of 60mg in a continuous dosing schedule. In the majority of cases, reduction to 40mg daily was required due to toxicity. However, cabozantinib has not been tested at lower doses for prolonged periods of time in our human trials. The clinical characteristics of the 21 patients enrolled in the phase 2 trial at MD Anderson Cancer Center are shown in Table S1. Patients were evaluated by bone scan and CT scan of the chest, abdomen, and pelvis every 6 weeks. Informed consent was obtained after the nature and possible consequences of the studies were explained. Of the 21 patients studied, 10 (48%) presented with an anaplastic phenotype. This phenotype is recognized as a lethal variant that often arises after multiple treatments and may be implicated in as many as 30% of prostate cancer-related mortality (12).

Human tissues

Blood and bone marrow specimens were obtained at baseline and after 6 weeks on cabozantinib. The half-life of cabozantinib is 59.1−136 hours, and steady-state blood concentration levels are achieved within approximately 3 weeks (13). Thus, by the time of the second biopsy, cabozantinib levels had reached steady state. Bone marrow specimens were obtained by transiliac biopsy. Nine matched cases (i.e. cases in which tumor-positive biopsies were obtained from the same patient before and after treatment) were analyzed for the parallel investigation.

Bone scan lesion area

Changes in bone metastases in patients after 6 weeks of cabozantinib treatment were quantified as changes in bone scan lesion area (BSLA) by using a computer-aided detection system described by Lee et al. (14). A bone scan response was defined as a ≥30% decrease in BSLA.

NaF-18 PET scanning

NaF-18 PET scanning of mice was done at baseline (at 12 days after the intrafemoral injection of MDA-PCa-118b PDX), and at 24 and 44 days after initiation of treatment. Images were obtained with an animal PET/CT scanner (Inveon, Siemens Healthcare). Details of the procedures and analysis of the images are provided in Supplemental Methods.

Cytokine array serum markers

Levels of cytokines and biomarkers in patient serum samples were measured by using the Aushon multiplex immunoassay platform (Aushon BioSystems, Billerica, MA), and data were analyzed with Aushon's PROarray Analyst Software.

Primary patient-derived prostate cancer xenografts

The development and characterization of primary xenograft models have been described elsewhere (15, 16). Between 2009–2012, 35 PDX models were developed from 96 attempted (36%). For this study, we used fresh frozen tumors from stock of PDX models that have been well characterized and represent different spectra of PCa progression. Briefly, the MDA PCa-180-30 xenograft has morphologic features of conventional adenocarcinoma and expresses high levels of AR. The MDA PCa-144-13 xenograft has morphologic features of mixed adenocarcinoma and small cell prostate cancer. The MDA PCa-118b xenograft when implanted in the mouse femur, exhibits a strong osteogenic phenotype similar to that of the human prostate cancer from which it was derived (17). Importantly, the MDA PCa-118b induces new bone formation even at subcutaneous sites (17, 18). Histologic analysis of subcutaneous MDA PCa-118b implants indicates that they have all of the cellular elements, including osteoblasts and osteoclasts, of human bone lesions (19).

Development of the sh-c-*met*-expressing MDA PCa-144-13 xenograft

To develop xenografts in which MET expression was reduced, a single-cell suspension of MDA PCa-144-13 cells from a fresh tumor was maintained in tissue culture plates for 3 days. Cells were infected with lentivirus directing the expression of sh-c-*met* or a non-targeting (NT) sequence (Supplemental Table 2). NT and sh-c-*met* MDA PCa-144-13 cells were sorted for green fluorescence protein and injected into the flanks of SCID mice.

Reagents

Cabozantinib (XL-184) is a small-molecule tyrosine kinase inhibitor that potently targets MET, VEGFR-2, and several other receptor tyrosine kinases implicated in tumor pathobiology, including RET, TIE2, AXL, FLT3, and KIT.[14] Cabozantinib was provided by Exelixis (South San Francisco, CA). For the parallel mouse experiments, cabozantinib was

formulated in sterile H_2O/10 mmol/L HCl. Antibodies used in the study are listed in Supplemental Table 3.

Treatment of MDA PCa-180-30, MDA PCa-118b, and MDA PCa-144-13 xenograft tumors

Primary xenograft experiments were performed in accordance with regulations and standards of the U.S. Department of Agriculture, the U.S. Department of Health and Human Services, the National Institutes of Health, and The University of Texas MD Anderson Cancer Center Institutional Animal Care and Use Committee guidelines. Mouse treatment schedules are described in the Supplemental Methods. Tumor volumes were calculated with the formula $V= (W/2)*(L)^2$. Mice were killed when tumor volume reached $1500mm^3$, when weight loss exceeded 30%, or at the times specified in the Results section. After the mice were killed, tissue samples were preserved for H&E staining, immunoblotting, immunohistochemical staining, and immunofluorescence staining as described elsewhere (16, 20, 21).

Statistical methods

Differences among groups were assessed by Student's *t* tests or analysis of variance (ANOVA) followed by Fisher's exact tests for multiple comparisons. Tumor growth was compared by repeated-measures ANOVA and survival by the log-rank (Mantel-Cox) test. *P* values <0.05 were considered significant. Error bars show means ± standard error of the mean (SEM). For human studies, descriptive statistics were used to summarize maximum changes in bone-specific alkaline phosphatase (BAP), urine N-telopeptides (uNTx), and cytokines that occurred during treatment.

Results

Responses to cabozantinib in a phase 2 clinical trial and PDX MDA PCa-118b grown intrafemurally

Sixteen of 20 patients in the phase 2 trial (80%) showed greater than a 30% reduction in Bone Scan Lesion Area (BSLA), a measure of tumor response, at six weeks after treatment (Figure 1A). Four representative bone scans are shown in Figure 1B -one from a non-responder, two from partial responders and one from a patient showing complete bone scan resolution. Patient characteristics are shown in Supplemental Table 1. To determine if the responses of PDX grown in the bone were consistent with what was observed in patients in the trial, we injected MDA PCa-118b (1×10^6 cells) into the femur of immunodeficient mice, and obtained baseline MRI scans 10 days later. After randomization of mice based on both tumor size and growth of tumor inside the bone, half the mice were treated with cabozantinib starting 10 days after the MRI, and the other half were treated with vehicle alone. Untreated tumors grew exponentially (as estimated by MRI), whereas tumor growth was strongly inhibited by cabozantinib. Representative MRI scans are shown Figure 1C (left panels). Tumor volumes (Figure 1C, right panel) were calculated as described in Materials and Methods.

Next, to examine bone turnover in mice, we used a functional bone imaging technique involving NaF-18 PET scans as described in Materials and Methods. Changes in signal

intensity in control bones were apparent in the PET (Figure 1D, left panel). The Standard Uptake Value (SUV-calculated as described in Materials and Methods) demonstrated decreased bone turnover in cabozantinib-treated mice relative to untreated mice (Figure 1D, right panel). Representative PET scans of whole mice including an intensity scale are shown in Supplemental Figure 1. These results demonstrate that responses to cabozantinib in the MDA PCa-118b intrafemoral model correspond with initial responses in the clinical trial.

Responses to cabozantinib in subcutaneous models mimic response to tumors growing in the bone

We next examined the effects of cabozantinib on the subcutaneous growth of MDA PCa-118b and two other PDX models -the AR-positive MBA-PCa 180-30 PDX and the AR-negative MDA PCa-144-13 (the latter two PDX can only be grown subcutaneously). Tumor stabilization was observed in all three PDX as estimated by tumor volume (Figure 2A-C) and was comparable to that observed in tumors grown intrafemurally. Relative growth in control and cabozantinib-treated mice was similar in each model (Supplemental Figure 2A-C). Animal weights were maintained throughout treatment (Supplemental Figure 2-D-F). Cabozantinib-treated mice also had a substantially prolonged survival time (i.e. time until tumor volume reached 1500mm^3) relative to control mice in each model (Supplemental Figure 2G-I). Thus, the results from xenograft models parallel the clinical responses of our patient population and of patients reported by others (6).

Although tumor volume was stabilized, massive tumor necrosis was observed in the PDX models after three weeks of cabozantinib treatment (Figure 2D). Occupancy of viable tumor cells was determined in the tumor mass (as measured by H&E in 10 tumor sections, 4× magnification) significantly decreased in all xenografts (Figure2D, quantified in 2E). Areas of necrosis exceeded 70% of total tumor section area (Figure 2E). Thus, these PDX studies demonstrated regression in tumor burden.

Furthermore, a characteristic pathologic finding in these PDX specimens after cabozantinib treatment was the presence of multiple, well-defined islets (80–160μm radius) of viable tumor cells with a central blood vessel. The patient studies included trans-iliac bone marrow biopsies collected at baseline and after six weeks of daily cabozantinib treatment. Similar-sized foci of viable tumor cells (65–150μm radius) were seen in both patient biopsies and in treated MDA PCa-118b tumors grown intrafemurally (Figure 2F and Supplemental Figure 3), as well as PDX grown subcutaneously (Figure 2G and Supplemental Figure 3). Cells in the islets were actively dividing at rates comparable to untreated tumors, as determined by phospho-histone H3 staining, (Figure 2H upper panel; H&E shown in insets; quantification shown in lower panel). Thus, residual, viable tumor cells were a common characteristic of patient samples and all xenograft models examined. A schematic representation of the features of islets is shown in Figure 2I.

MET activation persists in human and mouse tumors treated with cabozantinib

We next determined if cabozantinib inhibited MET phosphorylation in viable tumor cells. We performed IHC staining for total MET and activated p-MET on pre-treatment and cabozantinib-treated tumor specimens from both humans (after 6 weeks of daily

cabozantinib, when steady state levels of cabozantinib were achieved (13)) and mice after 3 weeks of treatment. Mice were sacrificed 2–4hrs after the final cabozantinib treatment. Bone scan images, Computer Tomography scans, H&E staining, MET and p-MET are shown for representative patients with partial improvement (Figure 3A) and complete improvements (Figure 3B) on bone scans. In all nine patients in which tumor was evident in pre- and post-treatment biopsies, p-MET expression was observed at baseline, although staining intensity was variable. Eight of those nine patients showed no decrease in MET phosphorylation in six-week biopsies relative to baseline biopsies. A 30% decrease in p-MET was observed in the ninth patient. In parallel, PET Scans, H&E staining, MET and p-MET stainings were performed for intrafemoral MDA PCa-118b PDX (Figure 3C). Images of the excised tumor, H&E, MET and p-MET staining for subcutaneously grown MDA PCa-180-30 tumors are shown in Figure 3D. Cabozantinib effectively controlled tumor growth in both PDX, and the treated MDA PCa-180-30 tumors appeared to be reduced in angiogenesis as gauged by their white appearance (Figure 3D); however, as was true for human specimens, p-MET staining was not inhibited in islets of viable tumor cells.

PDX reveal initial, but not sustained p-MET inhibition by cabozantinib

The unexpected presence of p-MET (by IHC) after cabozantinib treatment raised several possibilities: (1) the drug was not hitting the target; (2) inhibition of p-MET occurred only at earlier time points than tested in patients; (3) inhibition of p-MET was not required for sustained growth inhibition by cabozantinib. As part of our parallel approach, we evaluated the effect of cabozantinib on p-MET expression over time in MDA PCa-144-13 xenografts. Mice were sacrificed and tissue obtained at intervals that could not be done clinically: 0, 2, 4, 6, 9, and 21 days after cabozantinib treatment. Findings from H&E, MET and p-MET staining are shown in Supplemental Figure 4A. By IHC, p-MET was nearly completely inhibited within two days of treatment, indicating cabozantinib was capable of inhibiting one of its principal targets. Thus, initial inhibition of tumor growth may be due, in part, to p-MET inhibition in tumor cells. However, p-MET was readily detectable after 9 days of treatment (Supplemental Figure 4A). The unanticipated MET reactivation explains the presence of MET phosphorylation in the islets of viable cells identified after 21 days, in which MET was phosphorylated to the same level as in control tumors.

To further examine mechanisms of tumor inhibition, immunoblotting was performed on tissue lysates from PDX specimens (control and cabozantinib treated). These experiments were performed after 4 days of treatment, before extensive necrosis occurred. In the MDA PCa-144-13 tumors, both p-MET and p-VEGFR-2 were inhibited after treatment, as expected (Supplemental Figure 4B, left panel). Cabozantinib treatment also led to inhibition of phosphorylation of the downstream targets, c-Src and Akt, but not their expression (Supplemental Figure 4B, right panel). These results confirm that cabozantinib inhibited primary and downstream signaling intermediates at early times after treatment.

MET signaling is not required for sustained growth of prostate cancer cells *in vitro* and *in vivo*

We next determined the relevance of p-MET in the islets of viable cells that persisted after cabozantinib treatment. For this study, we short-term cultured MDA PCa-144-13 cells and

assessed the effect of cabozantinib on these cultures. Both intrinsic p-MET (Figure 4A), and HGF-induced p-MET (Figure 4B) were inhibited. Next, we infected cultured MDA PCa-144-13 cells with a lentivirus directing the expression of an sh-c-*met* or a Non-targeting (NT) sequence as described in Materials and Methods. Infecting MDA PCa-144-13 cells with an sh-c-*met* lentivirus resulted in more than 90% decreased expression of MET protein, as determined by immunoblotting (Figure 4C), and decreased c-*met* mRNA by 92%, as determined by qRT-PCR (Supplemental Figure 5). However, no change was observed in downstream signaling, including p-Akt, and pErk1/ 2 (Figure 4C). Knockdown of MET also had no effect on apoptosis, as determined by cleaved PARP (Figure 4C), or on proliferation (Figure 4D). We next examined the effect of cabozantinib on proliferation of MDA PCa-144-13 cells transfected with a non-targeting vector or sh-c-*met* vectors *in vitro*. As shown in Figure 4E, cabozantinib at 100nM, a concentration that completely inhibited MET phosphorylation, had no effect on proliferation of both NT and MET knockdown variants after 96h. Similarly, cabozantinib concentrations from 10nM to 1mM had no effect on proliferation of cells transfected with an NT vector (Figure 4F) or on sh-c-*met* knockdown cells (Figure 4G) relative to untreated controls after 96h. Therefore, lack of inhibition by cabozantinib suggests no “off-target” effectors of proliferation were affected in tumor cells in this dose range.

Cabozantinib is equally effective in inhibiting tumor growth when MET is knocked down in MDA PCa-144 cells

Decreased MET expression had no effect on the subcutaneous tumor growth of MDA PCa-144-13 cells (Figure 4H), even though MET expression in the tumors (by immunoblotting) remained below detectable levels when tumors reached the maximal size (Supplemental Figure 6A). We then examined the response of NT and sh-c-*met* knockdown xenografts to cabozantinib treatment. Cells were inoculated into mice and cabozantinib treatment was performed as described above. In both the NT and sh-c-*met* knockdown xenografts, cabozantinib inhibited tumor growth (Figure 4I and J), despite the >90% decreased MET expression in the sh-c-*met* knockdown xenografts, though the initial cabozantinib-induced inhibition of tumor growth in the sh-c-*met* knockdown xenografts was marginally less. These results suggest that the primary long-term effect of cabozantinib on tumor growth inhibition/regression was due to targets in the microenvironment.

Cabozantinib induces a sustained inhibition of MET phosphorylation in endothelial cells

In the MDA PCa-144-13 sh-c-*met* tumors, MET and p-MET staining is almost entirely confined to the mouse vasculature (Figure 4K and Supplemental Figure 6B); consistent with efficient knockdown of MET in tumor cells. The macroscopic appearance of both NT and sh-c-*met* cells was similar, with the characteristic white tumors (similar to those described in Figure 3D, right panel), an indication of inhibition of angiogenesis (Figure 4K). To further assess angiogenesis in NT and sh-c-*met*-derived tumors, we used immunofluorescence staining and confocal microscopy and observed reduction of vasculature in both tumor types. However, as described above, p-MET-positive vessels (derived from mouse) were observed in the sh-c-*met*-derived untreated tumors. The near-complete lack of MET expression in tumor cells allowed us to examine the effect of cabozantinib on p-MET in the vasculature. As shown in Figure 4K, lower right panel, p-MET was inhibited in the CD31+

cells, suggesting that cabozantinib inhibits p-MET in the endothelial cells for long time periods. However, after 120 days treatment when MDA PCa-144-13 are resistant to cabozantinib, p-MET is observed in some vessels, suggesting partial reactivation (Supplementary Figure 6C).

Anti-angiogenic effects precede induction of apoptosis in cabozantinib-treated xenografts

Previous preclinical studies have shown that cabozantinib has strong anti-angiogenic and pro-apoptotic effects (4, 22, 23). Our xenograft models allowed us to examine whether changes in vasculature and cellular apoptosis occurred simultaneously with p-MET and p-VEGFR-2 inhibition. For these studies, we performed CD31 immunofluorescence at baseline and after 2, 4, 6, 9 and 21 days of cabozantinib treatment. Figure 5A shows H&E staining (to show tumor structure), TUNEL (to examine extent of apoptosis), CD31 (to identify vasculature), and DAPI (to stain nuclei). We observed decreases in the vasculature by day 2, and these decreases continued throughout treatment (Figure 5A, bottom panels). In contrast, apoptosis was observed only after 6 days of treatment, and continued to increase thereafter. Quantification of changes in CD31 expression is shown in Figure 5B; and for TUNEL, Figure 5C. The spatial distribution of apoptotic cells changed over time: at 21 days of treatment, apoptosis occurred only at the periphery of the previously described islets, whereas cells in close proximity to the central vessel were TUNEL negative (Figure 5A, middle and bottom panels). These results suggest that cabozantinib treatment does not induce apoptosis in tumor cells in islets, in accord with the positive phospho-histone H3 cells observed in Figure 2H. However, the time-dependent changes in the CD31+, TUNEL+ cells indicate that cabozantinib continues to induce sustained apoptosis in endothelial cells outside of the islets. To examine the effects of cabozantinib specifically on VEGFR-2, we used immunofluorescence (VEGFR-2 + CD31 + DAPI) to test cells at baseline and at 21 days after cabozantinib treatment. As shown in Figure 5D and quantified in Figure 5E, most, but not all, CD31+ vessels in control tumors co-stained for VEGFR-2 (VEGFR-2-negative vessels are indicated with arrows). Central vessels in islets of viable cells are CD31+, VEGFR-2-, and p-MET- (see Figure 4G), suggesting that combined inhibition of p-MET and VEGFR-2 contributes to the anti-angiogenic effect of cabozantinib. Vessel density was also examined in biopsy samples from human bone metastases and MDA PCa-118b tumors (Figure 5F). Cabozantinib treatment decreased vessel density. Foci (islets) of tumor cells grew in proximity to vessels, similar to what was observed in subcutaneous PDX models. Quantification of changes in vessel density in both human biopsies and PDX is shown in Supplemental Figure 7. Assessment of VEGFR-2 in bone tissue from human biopsies was not possible because of non-specific staining observed in the human bone.

To indirectly assess changes in angiogenesis in tumors from patients in the Phase 2 clinical trial, we analyzed cytokine and angiogenic factors (CAF) in serum samples from 16 patients at baseline and after 6 weeks on cabozantinib. Soluble VEGFR-2 levels decreased and soluble VEGF levels increased, changes associated with an anti-angiogenic effect (24–26). Increases in soluble VEGF were observed in 69% of patients (median change 85.5%, range -37% to 1,700%) (Figure 5G). Reductions in soluble VEGFR-2 (Figure5H) occurred in 94% of patients (median change 53.5%, range -76% to 54%). The combination of decreased

vessel density and changes in serum markers are consistent with cabozantinib having an anti-angiogenic effect in patients on the clinical trial.

Cabozantinib effects on bone

To evaluate cabozantinib effects on bone formation and remodeling in the phase 2 clinical trial, we measured changes in serum levels of bone specific alkaline phosphatase (BAP), indicative of osteoblast activity, and urine N-Telopeptides (uNTx), a measure of osteoclast activity. Reductions in BAP levels occurred in 60% of patients (median change -15%, range -55% to 302%-Supplemental Figure 8A). Reductions in uNTx occurred in 78% of patients (median change -31%, range -90% to 40%-Supplemental Figure 8B). We also examined two other markers of bone turnover: osteoprotegerin, which increased in 81% of patients (Supplemental Figure 8C); and osteopontin, which decreased in 94% of patients (Supplemental Figure 8D). These changes in bone remodeling markers agree with the findings of the bone functional imaging studies done for patients and mice (Figure 1A,D). To further examine the effects of cabozantinib on bone formation, we performed microCT to visualize intrafemoral MDA PCa-118b PDX. We obtained high-resolution images directly comparing the tumor-bearing and contralateral femur in live animals at two time points-3 days before to treatment and 45 days after-treatment. Bone formation and destruction were observed in untreated tumors (Supplemental Figure 9A, upper and middle panels; compare tumor bearing right femur 45 days after treatment relative to femur at baseline), whereas bone structure was largely preserved in the cabozantinib-treated animals. Extra medullary bone formation was observed in 3 of 5 untreated mice (60%), and an increase in intramedullary bone formation was observed in all untreated mice (Supplemental Figure 9A lower panel). In contrast, no obvious increase in bone formation was observed in cabozantinib-treated mice (Supplemental Figure 9A). Quantitation of bone volume (Supplemental Figure 9B) and bone density (Supplemental Figure 9C) demonstrated no statistically significant difference in percent change after 45 days of treatment compared with baseline.

Further, to determine if cabozantinib had direct effects on osteoblasts, we examined the effects in primary mouse osteoblasts (PMOs) from newborn mouse calvaria. Cabozantinib treatment led to inhibition of osteoblast proliferation (Supplemental Figure 9D). When PMOs treated with cabozantinib were cultured in differentiation medium for 18 days, expression of alkaline phosphatase (Supplemental Figure 9E) and osteocalcin (Supplemental Figure 9F), both markers of osteoblast differentiation, were increased relative to untreated cells. These observations demonstrate that cabozantinib treatment directly affects osteoblasts, inhibiting their proliferation and inducing differentiation.

Continuous cabozantinib treatment is required to control tumor growth

An observation from the clinical trial was that in patients where therapy was discontinued due to toxicity, tumors rapidly progressed. We therefore used PDX models to determine if an intermittent approach were sufficient to sustain response or if continuous treatment were required for optimal response. For this experiment, mice with xenograft tumors were treated for 21 days and then randomly assigned to continuous treatment or withdrawal arms. In the continuously treated mice, minimal changes in tumor volume were observed for 50 days,

indicating that cabozantinib effectively inhibits xenograft growth for relatively long treatment periods. In contrast, cabozantinib withdrawal led to rapid, immediate exponential re-growth of all tumors (Figure 6A). These results demonstrate that continuous treatment is required to inhibit tumor regrowth. Next, we compared tissues stained for H&E, MET, p-MET and phospho-histone H3 from untreated and cabozantinib-withdrawal specimens. As shown in Figure 6B, p-MET expression and proliferation are nearly identical in these specimens. Phospho-histone H3 staining is quantified in Supplemental Figure 10.

Development of Acquired Resistance

Finally, we examined the effect of even longer cabozantinib treatment in the two PDX, MDA PCa-144-13. After ~120 days treatment, treated PDX grew exponentially in the presence of cabozantinib, at rates similar to untreated tumors. After re-implantation of tumors into SCID mice for three generations, resistance to cabozantinib was maintained (Figure 6C), and p-MET levels, as determined by IHC, were equivalent to those of untreated tumors (Figure 6D). Genomic sequencing showed no amplification or mutation of c-*met* in resistant tumors (data not shown).

Downregulation of MET signaling is associated with upregulation of FGFR-1 expression

Numerous reports have demonstrated that acquired resistance to tyrosine kinase inhibitors targeting growth factor receptors arises from overexpression or amplification of non-targeted receptor kinases that perform overlapping signaling (27–33). Therefore, we evaluated the expression of several growth factor receptors that might contribute to acquired cabozantinib resistance. Treatment with cabozantinib did not lead to substantial changes in the expression of IGF-1R, EGF-R or VEGFR-1 in tumor cells (data not shown), but did lead to increased expression of FGFR-1, as shown by immunoblotting (Fig. 6E) and immunohistochemistry (Figure 6F) in cabozantinib-resistant MDA PCa-144-13 tumors. To further determine whether MET inhibition led to increased FGFR-1 expression, we examined the effect of continuous cabozantinib treatment *in vitro* in the expression of these receptors. As shown in Figure 6G, treatment with cabozantinib for 4 weeks led to upregulation of FGFR-1 expression relative to untreated controls. In contrast, the expression of EGF-R was unchanged relative to untreated cells. Next, we examined FGFR-1 expression 10 days following MET knockdown in both 144-13 and PC3 cells. As shown in Figure 6H, the expression of FGFR-1 is significantly higher in MET knockdown cells relative to cells expressing the NT vector, with no change in EGFR or IGFR-1. Thus, inhibition of MET activity or expression corresponds to increased FGFR-1 expression in two PCa models *in vitro* and *in vivo*.

Discussion

Results from parallel studies of investigational therapeutic agents in well-characterized PDX and clinical trials can provide unanticipated insights into mechanisms of clinical efficacy and development of resistance. We applied this approach to studying the effects of cabozantinib, a multi-targeted p-MET, p-VEGFR-2 inhibitor that had promising activity in phase 1 and phase 2 clinical trials in prostate cancer. In a recent phase 3 trial in mCRPC, cabozantinib prolonged progression free but not overall survival (6, 14, 34–36). The

advantage of our parallel approach is that by using models of tumor growth in mice that closely mimic response in humans, mechanistic studies could be performed that lead to an understanding of therapeutically relevant targets, mechanisms of resistance and dosing schedules that affect the efficacy of targeted therapies that should dictate development of future clinical trials.

First, we showed that responses in PDX by pathology and radiographic imaging closely mimicked responses in human patients. In most patients and mice harboring PDX, cabozantinib treatment initially resulted in tumor stabilization or regression. However, we demonstrated in both human patients and PDX models that primary resistance occurs, as cabozantinib fails to inhibit tumor cell growth at physiologically relevant concentrations. This result is manifested in the presence of similar-sized islets of viable resistant tumor cells found in both PDX and in the phase 2 clinical trial. Strikingly, while p-MET is initially inhibited and may account for initial growth inhibition, these islets of resistant cells were p-MET positive, suggesting that MET phosphorylation is reactivated by an HGF-independent mechanism, as serum levels of the ligand for MET, HGF, remain unchanged. Several mechanisms have been reported for non-ligand induced MET activation that could account for these results (21, 22, 37–40).

To directly examine the role of p-MET in tumor growth and response to cabozantinib, we derived MDA PCa-144-13 xenografts in which MET expression was reduced by >90%. Surprisingly, downregulation of MET had no effect on MDA PCa-144-13 cell proliferation, either *in vitro* or *in vivo*. Similar conclusions regarding the role of MET in proliferation of SW1736 thyroid cancer cells were reached by Zhou et al., who transfected these cells with c-*met*-targeted siRNAs and demonstrated that neither cell cycle arrest nor apoptosis were observed *in vitro* (41). More strikingly, our studies demonstrated that in the near-complete absence of MET expression in xenografts, cabozantinib was equally effective in inhibiting tumor growth as in NT-infected cells with robust MET expression. In contrast to our studies, those of Dai et al., demonstrated that at concentrations of 2–5μM cabozantinib did lead to growth inhibition, but these concentrations are above what can be achieved clinically (42). Thus, the ability of cabozantinib to inhibit p-MET in the tumor cells appears unlinked from a sustained antitumor response, at least in established mCRPC. Our results agree with several clinical studies that demonstrate that inhibition of the HGF/MET axis alone has modest clinical benefit. Specifically, in mCRPC, the addition of monoclonal anti-MET antibodies to conventional chemotherapeutics failed to show significant increases in overall survival (43).

These results do not preclude a role for MET signaling in prostate cancer at earlier stages of progression. MET expression increases with prostate cancer stage, with the highest levels found in bone metastases (44); however, it should be noted that in primary tumors, expression and activation of MET did not correlate with disease recurrence (45, 46). An inverse correlation between AR activity and MET expression also has been described (47). Recently, Chu et al. demonstrated a feed-forward loop between RANK and MET, and in their studies, blocking MET expression inhibited the development of bone metastases after intracardiac injection (46). Thus, MET may play an important role in the establishment of metastases, but not in the continued growth of tumors once metastasis has occurred. Further,

studies in genetically engineered mouse models suggest that MET might be a therapeutic target when it is amplified in tumor cells (48). Thus, understanding at which stages of the disease MET may drive tumor progression will be critical to finding efficacy for drugs like cabozantinib that target this receptor tyrosine kinase.

Our results suggest that the mechanism of action of cabozantinib is primarily through microenvironment targeting, with VEGFR-2 being a principal target. Unlike p-MET in tumor cells, both p-VEGFR-2 and p-MET are inhibited long term in endothelial cells, corresponding with inhibition of angiogenesis in both patients from the phase 2 trial and in PDX. Numerous studies have shown that combining p-MET inhibition with p-VEGFR-2 inhibition is superior to anti-VEGF therapy alone (49, 50). This result supports studies demonstrating that inhibition of both MET and VEGFR-2 is superior in inhibiting vasculature to inhibiting either receptor alone (50, 51). However, our results provide insights as to how vascular heterogeneity contributes to the formation of islets of resistant cells. As observed in Figure 5, most tumor-associated vessels in untreated tumors were VEGFR-2-positive. However, islets of MET-positive tumor cells surrounded large VEGFR-2-negative vessels. Thus, the recognized heterogeneity of tumor-associated vasculature may account for the emergence of resistance to cabozantinib and other therapeutic agents that target VEGFR-2 (52), and islets of viable cells that grow in close proximity to mature vessels, which Dvorak and colleagues have shown to express low levels of VEGFR-2 and are therefore resistant to angiogenesis inhibitors (53). An alternative approach that may lead to improved tumor control is to add a vascular-targeting agent that would affect VEGFR-2-negative vessels to cabozantinib, to achieve a more complete vascular suppression.

Despite the profound inhibition of VEGFR-2+ vessels by cabozantinib, leading to tumor cell apoptosis and tumor volume stabilization, therapy withdrawal led to rapid and exponential growth of tumor cells. This characteristic re-growth of tumor cells has been associated with other angiogenesis-targeted agents, and as discussed above, was observed in patients on the Phase 2 clinical trial. This result is not surprising, as we demonstrate that residual tumor cells in the islets continue to proliferate at similar rates as control tumors. Thus, continuous exposure to cabozantinib that is sufficient to suppress angiogenesis may therefore be required to maximize its anti-tumor effect. This approach is in contrast to cabozantinib dosing strategies in medullary thyroid cancer where RET may be an important target (34, 54), that favor maximal tolerated doses and necessary imposition of rest periods when toxicity occurs. This result demonstrated an advantage to parallel use of PDX in conjunction with an early-stage clinical trial, and may account for the failure of the Phase 3 cabozantinib trial in prostate cancer, as many patients were withdrawn from therapy due to toxicity.

In addition to its effects on vasculature, cabozantinib directly affects bone formation and turnover. Decreases in serum alkaline phosphatase and urinary N-telopeptides, as found in the phase 2 clinical trial, are characteristic of inhibition of bone remodeling. In mice with intrafemoral MDA PCa-118b cells, cabozantinib caused a pronounced decrease in NaF-18 accumulation, consistent with reduced bone turnover, as was also observed by Graham et al. (23, 55). In our model, we were able to examine bone volume and density in the same animals before and at the end of treatment. Although we found no change in gross bone volume or density, intramedullary bone formation occurred only in untreated tumors. Viable

osteoblasts were observed in cabozantinib-treated MDA PCa-118b tumors. We therefore examined the effects of cabozantinib in PMOs and found that proliferation was decreased and differentiation was induced, as determined by increased osteocalcin and alkaline phosphatase expression. We speculate that cabozantinib-mediated prostate cancer cell death leads to reduction of prostate cancer-induced new bone formation. Our *in vitro* results on effects of cabozantinib on osteoblasts from mouse calvaria, in which proliferation was inhibited and differentiation was induced, demonstrate a direct effect of cabozantinib in osteoblasts, as was also shown by Dai et al.(23). These effects provide an explanation for the improvement in bone scans and reduction in bone pain observed in patients who respond to cabozantinib. For this reason, bone scan changes alone are not sufficient to predict an anti-tumor response.

Finally, our results provide further evidence that inhibition of a single growth factor receptor in tumor cells is rapidly compensated by de-repression of a growth factor receptor with overlapping function. We demonstrate, for the first time, that inhibition of either MET activity or expression leads to increased expression of FGFR-1. This result agrees with signaling network models described by Wagner et al. (56), who predicted increased abundance of an RTK might be induced by pharmacologic inhibition of another RTK within the same class/cluster. Of note, FGFR-1 and MET are grouped within the same cluster based on these signaling network models (56). Whether overexpression of FGFR-1 mediates acquired resistance to MET inhibition will require further study.

Our integration of clinical and murine studies, conducted in parallel, led to new insights about the effects of cabozantinib on mCRPC that could not be ascertained by either type of study in isolation, and demonstrate the power of this approach for future investigational agents. Our studies also suggest that the evolving concept of “co-clinical” trials should be expanded. As initially conceived by Pandolfi and colleagues (1), the co-clinical aspect constitutes the use of genetically engineered mice with driving mutations characteristic of the human tumor, or PDX derived from the same patients undergoing a clinical trial. Our results illustrate the power of integrating data sets from complex PDX to efficiently prioritize observations of interest. This cross-species iterative process gains strength when identical conclusions arise from complex PDX, thus reducing the inherent bias of commonly used models. Because the distance between cancer genotypes and clinical phenotypes remains large for informing clinical decisions, parallel investigations involving PDX representative of the spectrum of mCRPC may rapidly lead to more biologically informed clinical trials.

Supplementary Material

Refer to Web version on PubMed Central for supplementary material.

Acknowledgements

We acknowledge Dr. William Benedict for the expert scientific suggestions and critical reading of the manuscript. We also acknowledge Katerina Kaffes and Michel Keith for NaF-18 PET scan and μCT data acquisition and analysis. Finally, we acknowledge Dana Aftab (Exelixis, Inc) of providing cabozantinib for preclinical studies.

Financial Support: This work is supported by the National Cancer Institute (NCI) Grant No. P50 CA140388; a Prostate Cancer Foundation (PCF) Challenge award; a PCF Creativity Award; and The University of Texas MD Anderson Prostate Cancer Moon Shots Program (Logothetis CJ, Gallick GE); a PCF Young Investigator Award (Varkaris, A); a PCF Career Development Award (Efstathiou E), a UT Health Innovation for Cancer Prevention Research Pre-doctoral Fellowship, The University of Texas School of Public Health – Cancer Prevention and Research Institute of Texas grant #RP101503 (Gaur S), Cancer Prevention and Research Institute of Texas grant #RPO150282 (Gallick GE) and Cancer Center Support Grant (CA16672), and the Solon Scott III donor funds (PGC).

REFERENCES

1. Nardella C, Lunardi A, Patnaik A, Cantley LC, Pandolfi PP. The APL paradigm and the "co-clinical trial" project. Cancer Discov. 2011; 1:108–116. [PubMed: 22116793]
2. Chen Z, Cheng K, Walton Z, Wang Y, Ebi H, Shimamura T, et al. A murine lung cancer co-clinical trial identifies genetic modifiers of therapeutic response. Nature. 2012; 483:613–617. [PubMed: 22425996]
3. Wan X, Corn PG, Yang J, Palanisamy N, Starbuck MW, Efstathiou E, et al. Prostate cancer cell-stromal cell crosstalk via FGFR1 mediates antitumor activity of dovitinib in bone metastases. Sci Transl Med. 2014; 6:252ra122.
4. Yakes FM, Chen J, Tan J, Yamaguchi K, Shi Y, Yu P, et al. Cabozantinib (XL184), a novel MET and VEGFR2 inhibitor, simultaneously suppresses metastasis, angiogenesis, and tumor growth. Mol Cancer Ther. 2011; 10:2298–2308. [PubMed: 21926191]
5. Basch E, Autio KA, Smith MR, Bennett AV, Weitzman AL, Scheffold C, et al. Effects of Cabozantinib on Pain and Narcotic Use in Patients with Castration-resistant Prostate Cancer: Results from a Phase 2 Nonrandomized Expansion Cohort. Eur Urol. 2014; 67:310–318. [PubMed: 24631409]
6. Smith DC, Smith MR, Sweeney C, Elfiky AA, Logothetis C, Corn PG, et al. Cabozantinib in patients with advanced prostate cancer: results of a phase II randomized discontinuation trial. J Clin Oncol. 2013; 31:412–419. [PubMed: 23169517]
7. Exelixis. Exelixis Announces Results from the COMET-2 Pivotal Phase 3 Trial of Cabozantinib in Men With Metastatic Castration-Resistant Prostate Cancer. 2014. http://www.exelixis.com/investors-media/press-releases?cpurl=http%3A%2F%2Firexelixiscom/phoenixzhtml?c=120923%26p=irol-newsArticle%26ID=1993605%26highlight
8. Shah RB, Mehra R, Chinnaiyan AM, Shen R, Ghosh D, Zhou M, et al. Androgen-independent prostate cancer is a heterogeneous group of diseases: lessons from a rapid autopsy program. Cancer Res. 2004; 64:9209–9216. [PubMed: 15604294]
9. Swanton C. Intratumor heterogeneity: evolution through space and time. Cancer Res. 2012; 72:4875–4882. [PubMed: 23002210]
10. Fisher R, Pusztai L, Swanton C. Cancer heterogeneity: implications for targeted therapeutics. Br J Cancer. 2013; 108:479–485. [PubMed: 23299535]
11. Gerlinger M, Rowan AJ, Horswell S, Larkin J, Endesfelder D, Gronroos E, et al. Intratumor heterogeneity and branched evolution revealed by multiregion sequencing. N Engl J Med. 2012; 366:883–892. [PubMed: 22397650]
12. Aparicio AM, Harzstark AL, Corn PG, Wen S, Araujo JC, Tu SM, et al. Platinum-based chemotherapy for variant castrate-resistant prostate cancer. Clin Cancer Res. 2013; 19:3621–3630. [PubMed: 23649003]
13. Kurzrock R, Sherman SI, Ball DW, Forastiere AA, Cohen RB, Mehra R, et al. Activity of XL184 (Cabozantinib), an oral tyrosine kinase inhibitor, in patients with medullary thyroid cancer. J Clin Oncol. 2011; 29:2660–2666. [PubMed: 21606412]
14. Lee RJ, Saylor PJ, Michaelson MD, Rothenberg SM, Smas ME, Miyamoto DT, et al. A dose-ranging study of cabozantinib in men with castration-resistant prostate cancer and bone metastases. Clin Cancer Res. 2013; 19:3088–3094. [PubMed: 23553848]
15. Aparicio A, Tzelepi V, Araujo JC, Guo CC, Liang S, Troncoso P, et al. Neuroendocrine prostate cancer xenografts with large-cell and small-cell features derived from a single patient's tumor: morphological, immunohistochemical, and gene expression profiles. Prostate. 2011; 71:846–856. [PubMed: 21456067]

16. Tzelepi V, Zhang J, Lu JF, Kleb B, Wu G, Wan X, et al. Modeling a lethal prostate cancer variant with small-cell carcinoma features. Clin Cancer Res. 2012; 18:666–677. [PubMed: 22156612]
17. Li Z, Mathew P, Yang J, Starbuck M-W, Zurita AJ, Liu J, et al. Androgen receptor–negative human prostate cancer cells induce osteogenesis through FGF9-mediated mechanisms. J Clin Invest. 2008; 118:2697–2710. [PubMed: 18618013]
18. Lee YC, Cheng CJ, Bilen MA, Lu JF, Satcher RL, Yu-Lee LY, et al. BMP4 promotes prostate tumor growth in bone through osteogenesis. Cancer Res. 2011; 71:5194–5203. [PubMed: 21670081]
19. Lindner G, Schwarz C, Kneidinger N, Kramer L, Oberbauer R, Druml W. Can we really predict the change in serum sodium levels? An analysis of currently proposed formulae in hypernatraemic patients. Nephrol Dial Transplant. 2008; 23:3501–3508. [PubMed: 18723567]
20. Park SI, Zhang J, Phillips KA, Araujo JC, Najjar AM, Volgin AY, et al. Targeting SRC family kinases inhibits growth and lymph node metastases of prostate cancer in an orthotopic nude mouse model. Cancer Res. 2008; 68:3323–3333. [PubMed: 18451159]
21. Varkaris A, Gaur S, Parikh NU, Song JH, Dayyani F, Jin JK, et al. Ligand-independent activation of MET through IGF-1/IGF-1R signaling. Int J Cancer. 2013; 133:1536–1546. [PubMed: 23526299]
22. Sennino B, Ishiguro-Oonuma T, Wei Y, Naylor RM, Williamson CW, Bhagwandin V, et al. Suppression of tumor invasion and metastasis by concurrent inhibition of c-Met and VEGF signaling in pancreatic neuroendocrine tumors. Cancer Discov. 2012; 2:270–287. [PubMed: 22585997]
23. Dai J, Zhang H, Karatsinides A, Keller JM, Kozloff K, Aftab DT, et al. Cabozantinib inhibits prostate cancer growth and prevents tumor-induced bone lesions. Clin Cancer Res. 2013; 20:617–630. [PubMed: 24097861]
24. Bocci G, Man S, Green SK, Francia G, Ebos JM, du Manoir JM, et al. Increased plasma vascular endothelial growth factor (VEGF) as a surrogate marker for optimal therapeutic dosing of VEGF receptor-2 monoclonal antibodies. Cancer Res. 2004; 64:6616–6625. [PubMed: 15374976]
25. Ebos JM, Lee CR, Bogdanovic E, Alami J, Van Slyke P, Francia G, et al. Vascular endothelial growth factor-mediated decrease in plasma soluble vascular endothelial growth factor receptor-2 levels as a surrogate biomarker for tumor growth. Cancer Res. 2008; 68:521–529. [PubMed: 18199548]
26. Norden-Zfoni A, Desai J, Manola J, Beaudry P, Force J, Maki R, et al. Blood-based biomarkers of SU11248 activity and clinical outcome in patients with metastatic imatinib-resistant gastrointestinal stromal tumor. Clin Cancer Res. 2007; 13:2643–2650. [PubMed: 17473195]
27. Engelman JA, Zejnullahu K, Mitsudomi T, Song Y, Hyland C, Park JO, et al. MET amplification leads to gefitinib resistance in lung cancer by activating ERBB3 signaling. Science. 2007; 316:1039–1043. [PubMed: 17463250]
28. Troiani T, Martinelli E, Napolitano S, Vitagliano D, Ciuffreda LP, Costantino S, et al. Increased TGF-alpha as a mechanism of acquired resistance to the anti-EGFR inhibitor cetuximab through EGFR-MET interaction and activation of MET signaling in colon cancer cells. Clin Cancer Res. 2013; 19:6751–6765. [PubMed: 24122793]
29. Vazquez-Martin A, Cufi S, Oliveras-Ferraros C, Torres-Garcia VZ, Corominas-Faja B, Cuyas E, et al. IGF-1R/epithelial-to-mesenchymal transition (EMT) crosstalk suppresses the erlotinib-sensitizing effect of EGFR exon 19 deletion mutations. Sci Rep. 2013; 3:2560. [PubMed: 23994953]
30. Meyer AS, Miller MA, Gertler FB, Lauffenburger DA. The receptor AXL diversifies EGFR signaling and limits the response to EGFR-targeted inhibitors in triple-negative breast cancer cells. Sci Signal. 2013; 6:ra66. [PubMed: 23921085]
31. Ware KE, Hinz TK, Kleczko E, Singleton KR, Marek LA, Helfrich BA, et al. A mechanism of resistance to gefitinib mediated by cellular reprogramming and the acquisition of an FGF2-FGFR1 autocrine growth loop. Oncogenesis. 2013; 2:e39. [PubMed: 23552882]
32. Bachleitner-Hofmann T, Sun MY, Chen CT, Tang L, Song L, Zeng Z, et al. HER kinase activation confers resistance to MET tyrosine kinase inhibition in MET oncogene-addicted gastric cancer cells. Mol Cancer Ther. 2008; 7:3499–3508. [PubMed: 18974395]

33. Chang J, Wang S, Zhang Z, Liu X, Wu Z, Geng R, et al. Multiple receptor tyrosine kinase activation attenuates therapeutic efficacy of the fibroblast growth factor receptor 2 inhibitor AZD4547 in FGFR2 amplified gastric cancer. Oncotarget. 2015; 6:2009–2222. [PubMed: 25576915]
34. Elisei R, Schlumberger MJ, Muller SP, Schoffski P, Brose MS, Shah MH, et al. Cabozantinib in progressive medullary thyroid cancer. J Clin Oncol. 2013; 31:3639–3646. [PubMed: 24002501]
35. Posadas EM, Figlin RA. Understanding the role of MET kinase in cancer therapy. J Clin Oncol. 2013; 31:169–170. [PubMed: 23213104]
36. Vaishampayan U. Cabozantinib as a novel therapy for renal cell carcinoma. Curr Oncol Rep. 2013; 15:76–82. [PubMed: 23292795]
37. Breindel JL, Haskins JW, Cowell EP, Zhao M, Nguyen DX, Stern DF. EGF receptor activates MET through MAPK to enhance non-small cell lung carcinoma invasion and brain metastasis. Cancer Res. 2013; 73:5053–5065. [PubMed: 23794705]
38. Dulak AM, Gubish CT, Stabile LP, Henry C, Siegfried JM. HGF-independent potentiation of EGFR action by c-Met. Oncogene. 2011; 30:3625–3635. [PubMed: 21423210]
39. Lu KV, Chang JP, Parachoniak CA, Pandika MM, Aghi MK, Meyronet D, et al. VEGF inhibits tumor cell invasion and mesenchymal transition through a MET/VEGFR2 complex. Cancer Cell. 2012; 22:21–35. [PubMed: 22789536]
40. Aftab DT, McDonald DM. MET and VEGF: synergistic targets in castration-resistant prostate cancer. Clin Transl Oncol. 2011; 13:703–709. [PubMed: 21975330]
41. Zhou Y, Zhao C, Gery S, Braunstein GD, Okamoto R, Alvarez R, et al. Off Target Effects of c-MET Inhibitors on Thyroid Cancer Cells. Mol Cancer Ther. 2013
42. Dai J, Zhang H, Karatsinides A, Keller JM, Kozloff KM, Aftab DT, et al. Cabozantinib inhibits prostate cancer growth and prevents tumor-induced bone lesions. Clin Cancer Res. 2014; 20:617–630. [PubMed: 24097861]
43. Ryan CJ, Rosenthal M, Ng S, Alumkal J, Picus J, Gravis G, et al. Targeted MET inhibition in castration-resistant prostate cancer: a randomized phase II study and biomarker analysis with rilotumumab plus mitoxantrone and prednisone. Clin Cancer Res. 2013; 19:215–224. [PubMed: 23136195]
44. Knudsen BS, Gmyrek GA, Inra J, Scherr DS, Vaughan ED, Nanus DM, et al. High expression of the Met receptor in prostate cancer metastasis to bone. Urology. 2002; 60:1113–1117. [PubMed: 12475693]
45. Jacobsen F, Ashtiani SN, Tennstedt P, Heinzer H, Simon R, Sauter G, et al. High c-MET expression is frequent but not associated with early PSA recurrence in prostate cancer. Exp Ther Med. 2013; 5:102–106. [PubMed: 23251249]
46. Chu GC, Zhau HE, Wang R, Rogatko A, Feng X, Zayzafoon M, et al. RANK- and c-Met-mediated signal network promotes prostate cancer metastatic colonization. Endocr Relat Cancer. 2014; 21:311–326. [PubMed: 24478054]
47. Verras M, Lee J, Xue H, Li TH, Wang Y, Sun Z. The androgen receptor negatively regulates the expression of c-Met: implications for a novel mechanism of prostate cancer progression. Cancer Res. 2007; 67:967–975. [PubMed: 17283128]
48. Wanjala J, Taylor BS, Chapinski C, Hieronymus H, Wongvipat J, Chen Y, et al. Identifying actionable targets through integrative analyses of GEM model and human prostate cancer genomic profiling. Mol Cancer Ther. 2015; 14:278–288. [PubMed: 25381262]
49. Sennino B, McDonald DM. Controlling escape from angiogenesis inhibitors. Nat Rev Cancer. 2012; 12:699–709. [PubMed: 23001349]
50. You WK, Sennino B, Williamson CW, Falcon B, Hashizume H, Yao LC, et al. VEGF and c-Met blockade amplify angiogenesis inhibition in pancreatic islet cancer. Cancer Res. 2011; 71:4758–4768. [PubMed: 21613405]
51. Sennino B, Ishiguro-Oonuma T, Schriver BJ, Christensen JG, McDonald DM. Inhibition of c-Met reduces lymphatic metastasis in RIP-Tag2 transgenic mice. Cancer Res. 2013; 73:3692–3703. [PubMed: 23576559]

52. Sitohy B, Nagy JA, Jaminet SC, Dvorak HF. Tumor-surrogate blood vessel subtypes exhibit differential susceptibility to anti-VEGF therapy. Cancer Res. 2011; 71:7021–7028. [PubMed: 21937680]

53. Sitohy B, Nagy JA, Dvorak HF. Anti-VEGF/VEGFR therapy for cancer: reassessing the target. Cancer Res. 2012; 72:1909–1914. [PubMed: 22508695]

54. Postel-Vinay S, Schlumberger M, Soria JC. Tumour markers fluctuations in patients with medullary thyroid carcinoma receiving long-term RET inhibitor therapy: ordinary lapping or alarming waves foreshadowing disease progression? Ann Oncol. 2013; 24:2201–2204. [PubMed: 23986546]

55. Graham TJ, Box G, Tunariu N, Crespo M, Spinks TJ, Miranda S, et al. Preclinical evaluation of imaging biomarkers for prostate cancer bone metastasis and response to cabozantinib. J Natl Cancer Inst. 2014; 106:dju033. [PubMed: 24634505]

56. Wagner JP, Wolf-Yadlin A, Sevecka M, Grenier JK, Root DE, Lauffenburger DA, et al. Receptor tyrosine kinases fall into distinct classes based on their inferred signaling networks. Sci Signal. 2013; 6:ra58. [PubMed: 23861540]

Statement of translational relevance

By integrating clinical and murine investigations, mechanisms of action of therapeutic agents can be linked to clinical benefit and development of resistance. Using this approach, we demonstrate that the clinical activity of cabozantinib, a multi-targeted MET/ VEGFR-2 inhibitor, is due primarily to inhibition of angiogenesis and bone turnover. We show that MET-positive tumor cells are present in both bone biopsies from responsive patients and patient-derived xenografts, and from the latter, that MET expression does not affect activity of cabozantinib. Further, we demonstrate that vascular heterogeneity represents one source of primary resistance to cabozantinib, and induction of FGFR-1 expression in tumor cells is a potential mechanism of acquired therapy resistance. Finally, we show that dosing schedule affects the efficacy of microenvironment targeting agents, such as cabozantinib. Our results provide general insights into targets and mechanisms of resistance that should dictate future development of clinical trials with targeted therapies.

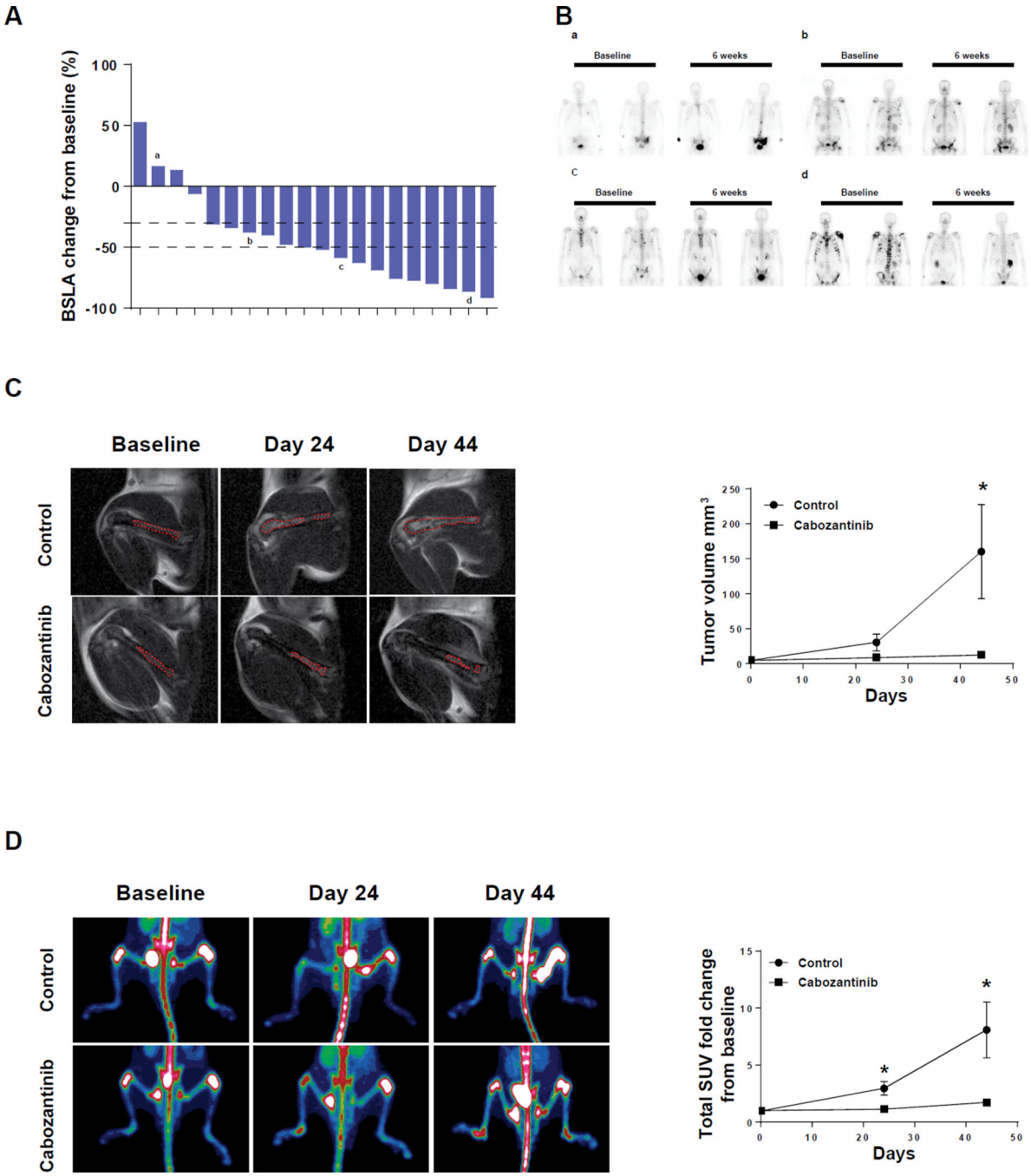

Figure 1. Cabozantinib activity in patients with mCRPC and PDX grown intrafemurally

(A) Quantitation of patients' BSLA changes at six weeks after cabozantinib treatment relative to baseline; (B) Representative Technetium-99 bone scan images of patients at baseline and six weeks after cabozantinib treatment; (a) no response; (b) partial response; (c and d) complete response; (C) Magnetic Resonance Imaging on cabozantinib-treated and control MDA PCa-118b PDX grown intrafemurally. Cells were injected into the femur, allowed to establish tumors and then treated as described in Materials and Methods. Tumor-bearing leg (tumors outlined in red) in control and treated animals were compared at

indicated times. Right panel: quantitation of tumor volume (*p<0.05); (D) NaF-18 PET scans on the same animals shown in (C). Right panel: quantitation of Standard Uptake Value as calculated by Inveon Research Workplace (*p<0.05).

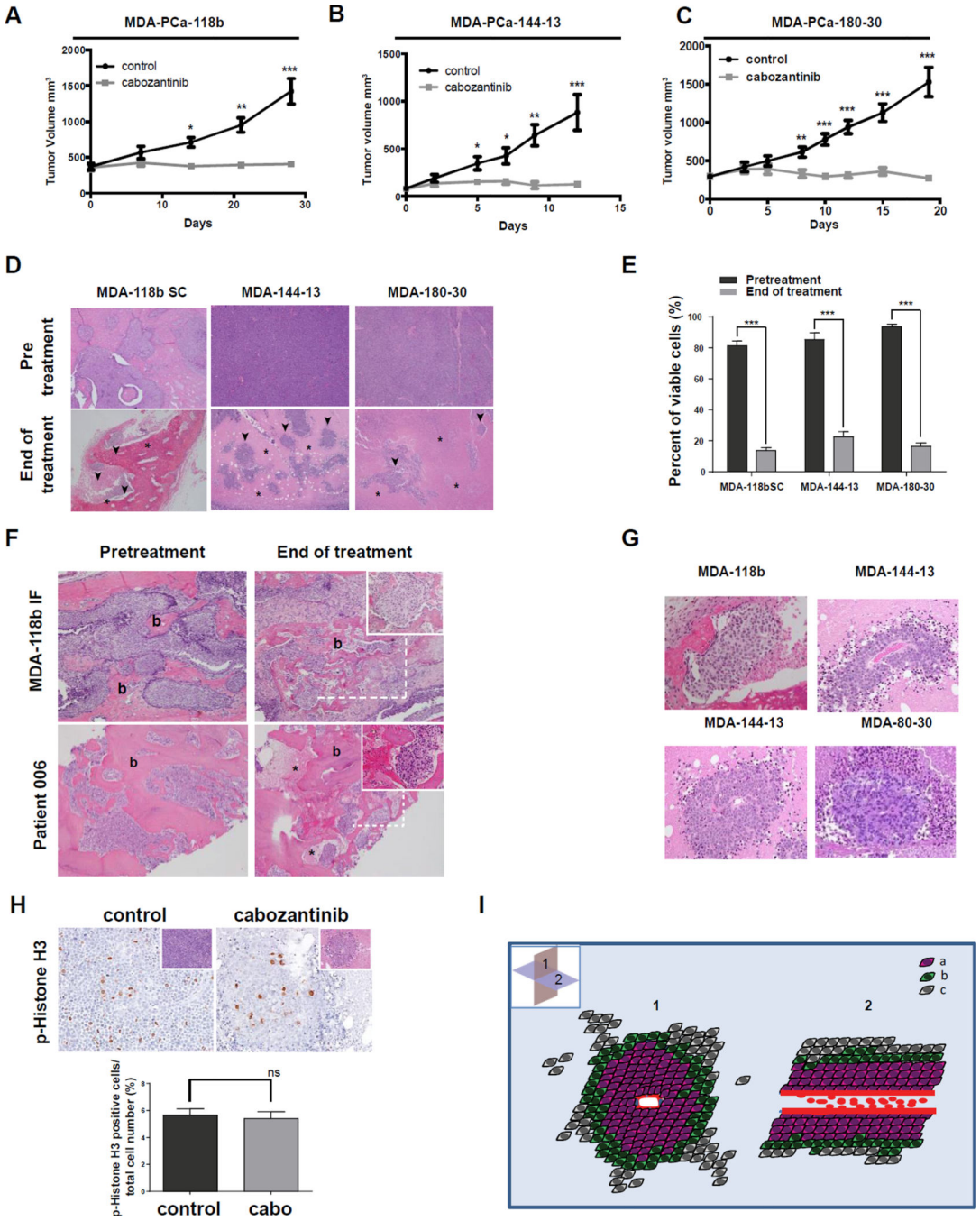

Figure 2. Growth Inhibition and Tumor islets of viable cells following Cabozantinib treatment in xenografts and human bone metastases

Xenograft tumors were grown subcutaneously to 100–400mm^3, and mice were randomized to vehicle-treated and cabozantinib-treated groups. (A), (B), (C) Growth of PDX treated 6 days/week by oral gavage with 30mg/kg cabozantinib or H_2O for indicated times (*p<0.01; **p<0.001; ***p<0.0001); (D) Representative H&E (4×magnification) of above xenograft tumors before and after 3–4 weeks of cabozantinib treatment; asterisks indicate necrotic areas; arrows indicate live tumor cells; b indicates bone; live tumor cells- (^); (E) Quantitation of occupancy of tumor mass by viable tumor cells at baseline and after 3 weeks

of cabozantinib treatment; (F) H&E showing bone-(b), necrotic tumor cells-(*) in MDA PCa-118b xenograft model (upper panels) and human bone metastases (lower panels) at baseline and end of cabozantinib treatment; (G) Islets of viable tumor cells in cabozantinib-treated tumors after 3 weeks (20×magnification); (H) H&E and phospho-histone H3 immunohistochemistry in control and cabozantinib treated tumor islets after 3 weeks (20×magnification); lower panel-quantitation of phospho- histone H3 staining. Inset- H&E staining of the same area. Graph shows the percentage of phospho-histone H3-positive cells relative to total number of viable cells (data represent mean and SEM); (I) Diagrammatic representation of islets: (a) live cells growing in proximity to the central vessel; (b) live cells on the periphery of the islet; (c) apoptotic and necrotic cells; (1) axial plane; (2) coronal plane showing red blood cells in center of islet.

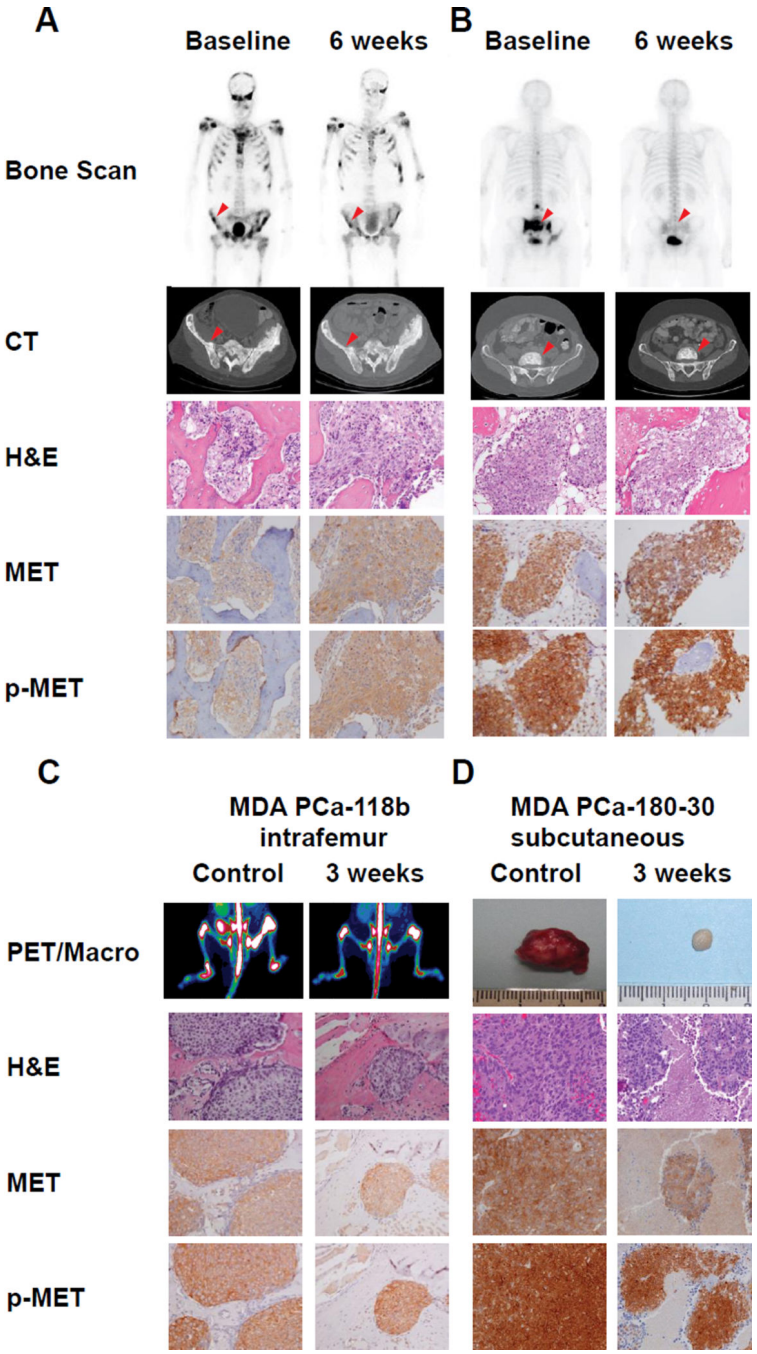

Figure 3. Response to Cabozantinib and MET Activation in Human Tumors and Primary Derived Xenografts

Bone scan, CT scan, H&E staining, and MET and p-MET IHC for mCRPC patients at baseline and six weeks after cabozantinib treatment for a patient with (A) partial response, and (B) complete response. Arrows indicate area of bone biopsy; (C) Response in MDA PCa-118b grown in the bone or (D) grown subcutaneously. **Left Panel**-PET scan of bone tumors; **Right panel**- macroscopic appearance for subcutaneously grown tumors; **Panels below**-H&E staining, MET and p-MET IHC.

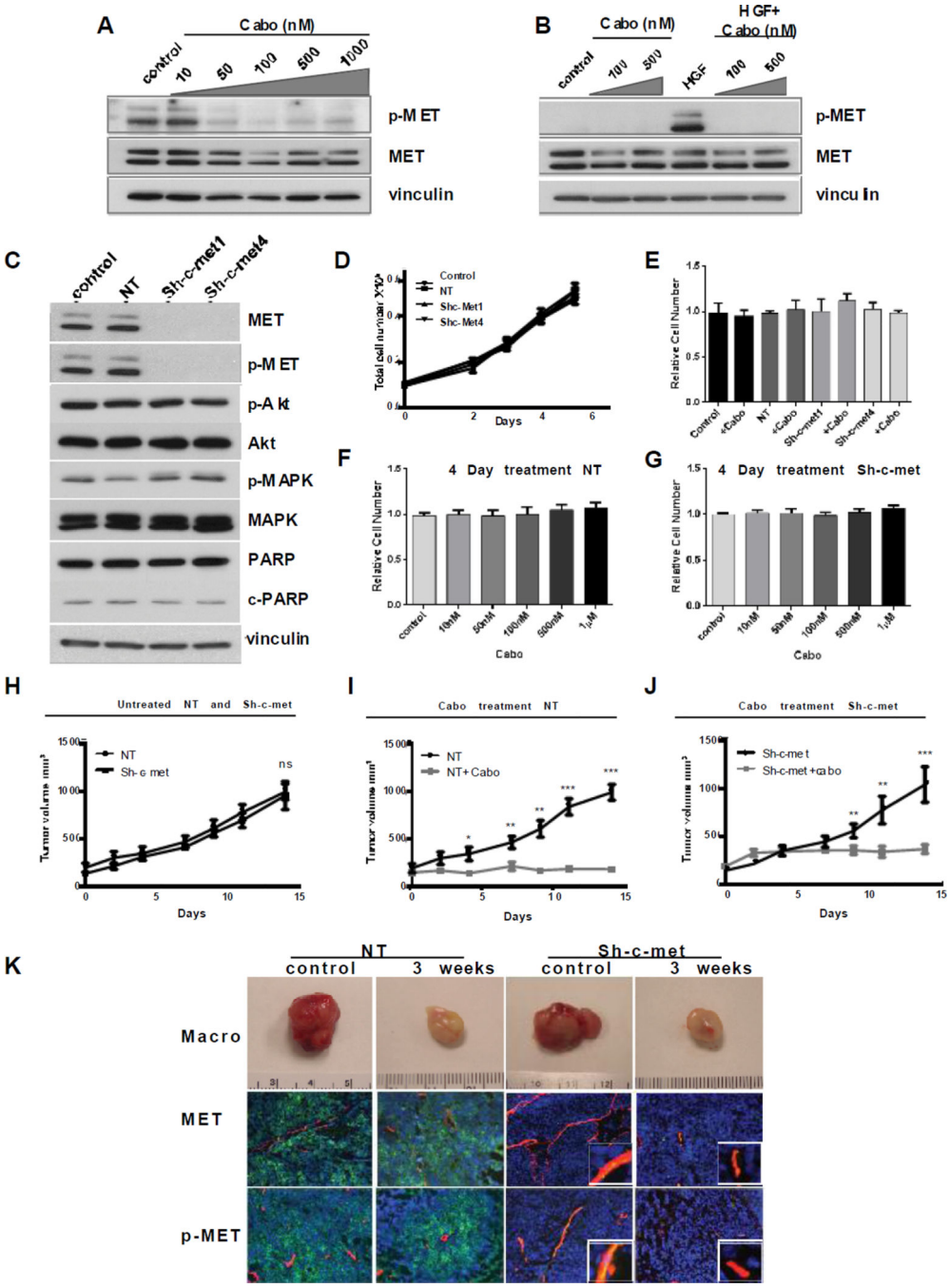

Figure 4. Role of p-MET in Cabozantinib Inhibition of Xenograft Growth

(A) MDA-PCa-144-13 cells were treated with cabozantinib at indicated concentrations for 2h. Expression and phosphorylation of MET were determined by immunoblotting; (B) MDA PCa-144-13 cells were pre-treated with cabozantinib for 2h and then stimulated with HGF (15ng/ml) for 10 min. Expression and phosphorylation of MET were determined by immunoblotting; (C) Expression and phosphorylation of MET and "downstream" targets in NT and sh-c-*met*-expressing cells. (D) In vitro proliferation of MDA PCa-144-13 control, NT, sh-*c-met1* and sh-*c-met4* cells. (E) The effect of cabozantinib (100nM) on proliferation

of parental, NT-transfected and sh-*met* transfected MDA PCa-144-13 cells; Dose-dependence effect of cabozantinib on proliferation (4 days) of (F) NT cells and (G) sh-c-*met* cells. (H) Growth of NT and sh-c-*met* expressing MDA PCa-144-13 tumors in mice. (I) Growth of NT xenograft tumors and (J) sh-c-*met* xenograft tumors treated 6 days/week by oral gavage with 30mg/kg cabozantinib or vehicle for indicated times (*$p<0.01$; **$p<0.001$. ***$p<0.0001$). (K) Effect on cabozantinib treatment on vasculature of NT and sh-c-*met* MDA PCa-144-13 tumors. **Upper panel**-macroscopic appearance of tumors; **Middle panel**-confocal microscopy of immunofluorescence staining MET-green/CD31-red/DAPI-blue; **Lower panel**- confocal microscopy of immunofluorescence staining p-MET (green)/ CD31(red)/DAPI(blue).

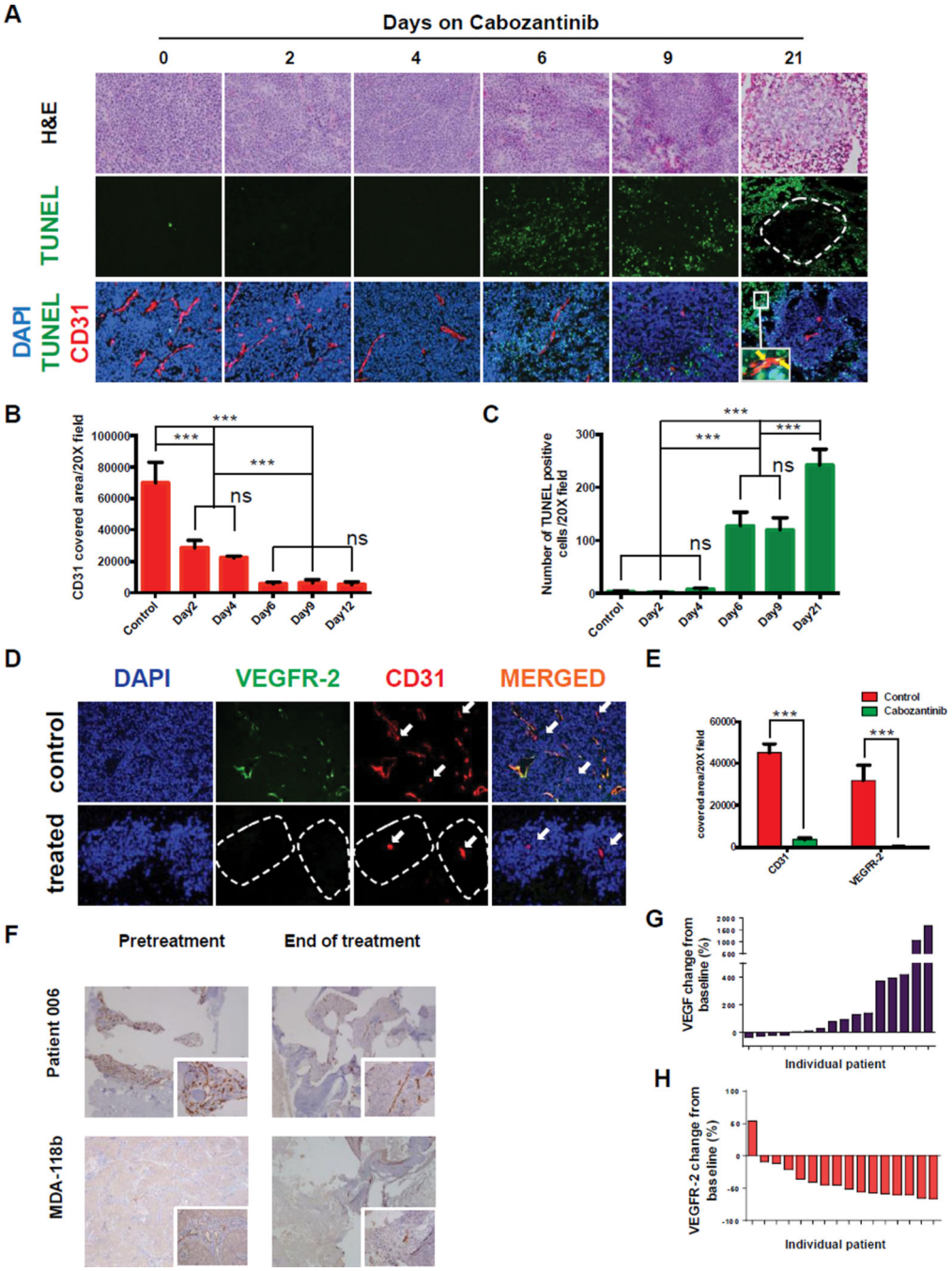

Figure 5. Effects of Cabozantinib on tumor vasculature

(A) Time-dependent cabozantinib-induced changes in vasculature and apoptosis in MDA PCa-144-13 xenograft models. Inset (lower right panel) indicates CD31-positive cells undergoing apoptosis (arrows). Broken line indicates border between islets of viable cells and TUNEL-positive cells; (B) quantitation of CD31 staining; (C) quantitation of TUNEL staining; values shown are mean and SEM; (ns–not statistically significant; **p<0.001; ***p<0.0001). (D) Confocal microscopy showing immunofluorescence of DAPI, VEGFR-2, and CD31 in control and cabozantinib-treated MDA PCa-144-13 tumors- arrows indicate

CD31 positive, VEGFR-2 negative vessels. Broken line indicates borders of the islets; (E) Quantitation of CD31 and VEGFR-2 immunofluorescence (data represent mean and SEM, ***$p<0.0001$); (F) Changes in tumor vasculature in MDA-118b model (upper panels) and human bone metastases (lower panels)-insets 20X magnification. Changes in angiogenesis markers in the serum of patients 6 weeks after cabozantinib treatment relative to baseline for (G) VEGF; (H) VEGFR-2.

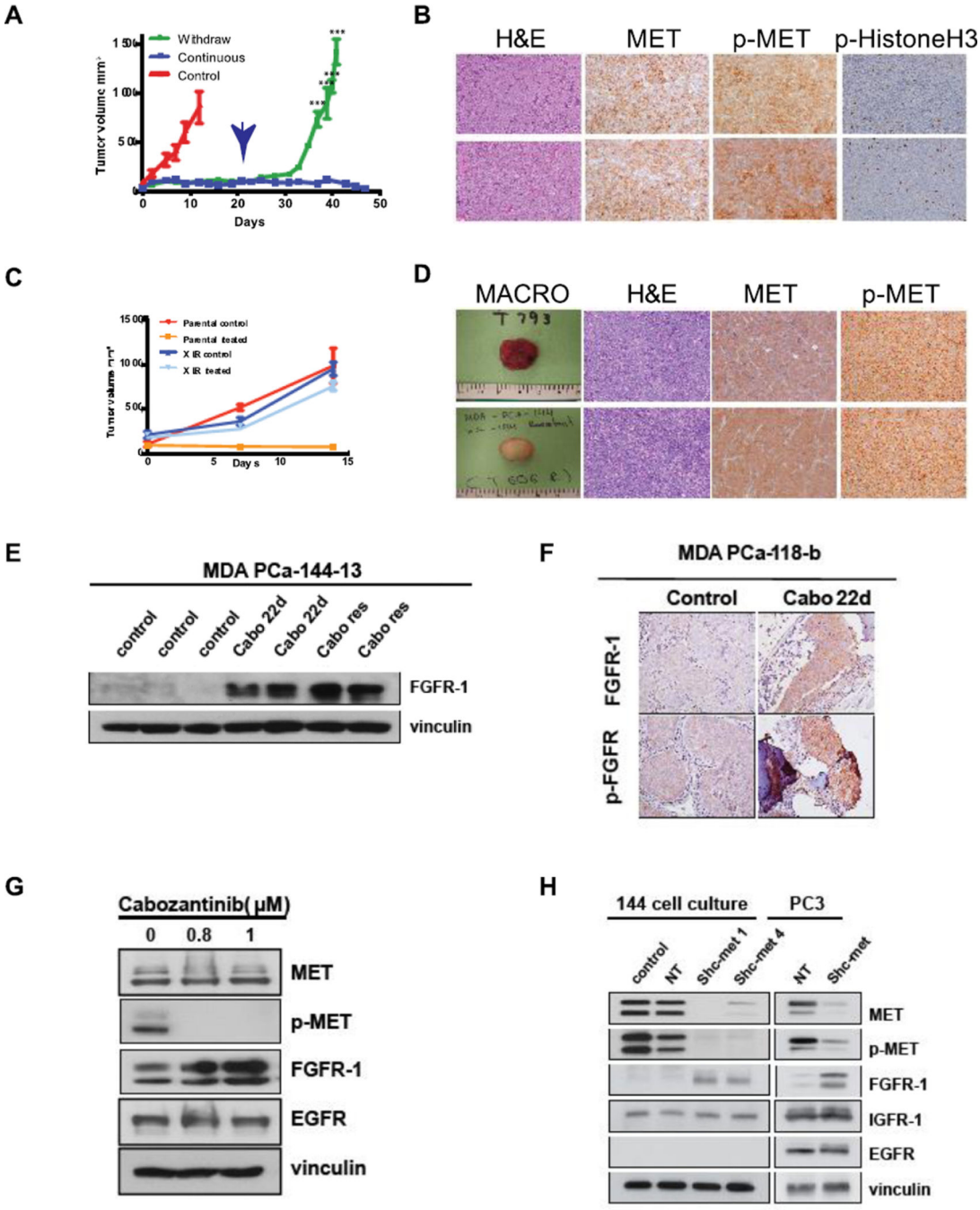

Figure 6. Acquired resistance to MET inhibition is associated with increased FGF-R1 expression

MDA-PCa-144-13 tumors were treated with cabozantinib for 21 days, then randomized to continuous treatment and withdrawal groups. (A) Tumor volume of continuously treated and withdrawal tumors (time of treatment withdrawal is indicated by the arrow). (B) H&E staining, MET, p-MET and phospho-histone H3 IHC in control tumors and tumors after cabozantinib withdrawal for 42 days; (C) Proliferation of parental and cabozantinib-resistant (XLR) tumors in the presence and absence of cabozantinib; (D) Macroscopic appearance, H&E, MET and p-MET staining of MDA PCa-144-13 XLR tumors in the presence and

absence of cabozantinib; (E) Immunoblot for FGFR-1 expression of MDA PCa-144-13 lysates from control, 22 day-treated and cabozantinib resistant tumors. (F) Immunohistochemistry of FGFR-1 expression after 22 days cabozantinib treatment in MDA PCa-118b PDX. (G) Immunoblot of MDA PCa-144-13 cells lysates treated continuously for 4 weeks with cabozantinib *in vitro*. (H) Immunoblot of MDA PCa-144-13 and PC3 parental, NT-transfected and sh-*met* transfected cells 10 days time after knockdown.